ELSEVIER

Journal of Photochemistry and Photobiology A: Chemistry 125 (1999) 13–19

Journal of Photochemistry and Photobiology A:Chemistry

Nanojoules, nanoliters and nanosecond calorimetry

Tom Autrey*, Nancy Foster, Kim Klepzig

Environmental and Health Sciences Division, Chemical Sciences Department, Pacific Northwest National Laboratory, POB 999, Richland, WA 99352, USA

Received 3 December 1998; received in revised form 11 February 1999; accepted 22 February 1999

Abstract

A nano-scale time-resolved calorimetric experimental approach is described using a photoacoustic cell made from narrow-bore flexible fused-silica capillary tubing. The fused silica capillary permits the transmission of an excitation source from the deep UV to the near infrared. Methods to couple the excitation energy into the sample and the acoustic energy away from the sample to the detector are discussed. To demonstrate the unique capabilities of the fused silica capillary cell, the excited triplet state energy (E_t) and lifetime (τ) of benzophenone (Bp) in the presence and absence of a quencher was measured. Irradiation of an air-saturated acetonitrile solution of Bp in the nano-scale photoacoustic cell, (i.e., absorption of ca. 100 nJ in a sample volume of 30 nl), yielded $E_t = 69.5 \pm 1.4$ kcal/mol and a τ of a few hundred nanoseconds. In the presence of potassium iodide (KI), a Bp^{*3} quencher, the lifetime was significantly reduced. The rate of triplet quenching by KI ($k_q = 3.9 \pm 0.2 \times 10^9\ M^{-1}\ s^{-1}$) was determined from the slope of the Stern–Volmer plot of l/τ observed versus quencher concentration.

Keywords: Photoacoustic; Time-resolved; Nanoscale; Capillary

Introduction

Time-resolved photoacoustic (PA) calorimetry provides an experimental method to measure both thermochemical and kinetic properties of photo-generated reactive intermediates [1–9]. Deconvolution methods have been successfully used to measure the lifetime of transient intermediates ranging from nanoseconds to microsecond [10–13]. In addition to the inherent sensitivity provided by PA methods [14–16], the ability to perform experimental measurements on infinitely small sample volumes is possible. Unlike conventional spectrophotometric techniques where the observed signal is proportional to the sample pathlength, the PA signal is proportional to the density of absorbed energy. The ability to measure a PA signal for minute sample volumes is due to the nature of the acoustic properties arising from the absorption of light and the detection of the transient pressure change, which occurs from both thermal and molecular volume changes, with ultrasonic piezoelectric transducers.

Several benefits including nanoliter sized samples and high-pressure experiments will result from a miniaturized time-resolved calorimetric PA 'experiment' e.g., reduced to the size of a narrow-bore (100–180 μm ID) flexible fused silica capillary (FFSC). The geometry of the PA sample cell and the volume of sample required for analysis is dictated by the ability to couple the light into the sample (uniform excitation without pyroelectric artifacts from scattered light) and the ability to couple the transient pressure change induced in the sample to the piezoelectric detector (optimizing the acoustic energy transfer across the various impedance layers comprising the cell). In the classical cuvette PA cell geometry, where the excitation beam propagates perpendicular to the transducer, milliliters of a sample solution are required for detection of a PA signal. The volume of sample necessary to obtain a PA signal was significantly reduced (to tenths of milliliter) with the introduction of the front-faced design (FFD) [17] and the layered prism cell (LPC) [18] accompanied by an increase in sensitivity. However none of these cells, cuvette, FFD or LPC, take full advantage of the low volume capabilities of PA spectrophotometry and all three are limited to experiments near ambient pressures. In addition to the obvious benefit of the minute sample size requirements required by the FFSC, advantages include an additional thermal detection method for capillary electrophoresis [19]. Our foremost interest lies in the ability to control the pressure in FFSC tubing between ambient and 60,000 PSI. For example, the dynamics of ethylene, hydrogen, carbon dioxide and carbon monoxide exchange from organometallic complexes have been examined by high pressure NMR spectroscopy using FFSC [20]. While other spectroscopic techniques have successfully employed high-pressure apparatus to examine the kinetics

*Corresponding author. Tel.: +1-509-375-3792; fax: +1-509-375-2186.

1010-6030/99/$ – see front matter
PII: S1010-6030(99)00054-4

of photo-generated meta-stable intermediates, to our knowledge little has been reported using high-pressure time-resolved PA studies[1] [21,22]. Given the simplicity of the FFSC high-pressure apparatus and the sensitivity of PA methods, in principle, the narrow bore flexible fused silica capillary tubing should be able to provide an experimental approach to perform time-resolved calorimetric experiments at pressures ranging from ambient up to 60,000 PSI.

The goal of this investigation was to devise an approach to employ narrow-bore FFSC tubing (e.g., 100–180 μm ID, 360 μm OD) as the PA sample chamber and to determine if time-resolved PA experiments are possible under ambient pressures. Specifically if the flexible capillary can be incorporated into a geometry that yields a method to (1) couple the pulsed laser into the sample and (2) couple acoustic signal from the sample to an ultrasonic transducer, a small volume (submicroliter) PA cell that would permit the transmission of an excitation source from the deep UV to the near infrared with potential high pressure capabilities could be realized.

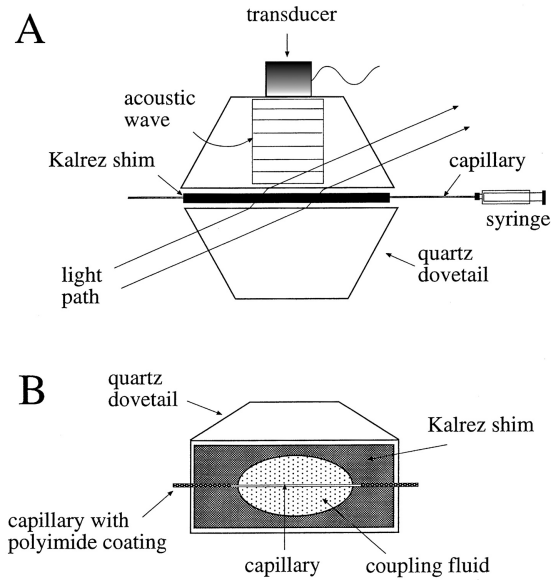

Fig. 1. Schematic representation showing the coupling of the excitation energy into and the acoustic energy away from the FFSC cell housed within the layered prism cell. Fig. 1(B) provides a side view cut away.

1. Experimental

1.1. Materials

The solvents, reagent grade, were obtained from Aldrich and used as received. Benzophenone (Bp) and *o*-hydroxybenzophenone (OHB) were obtained from Aldrich and then recrystallized from methanol.

1.2. Excitation sources and electronics

The fundamental line of a Nd:Yag laser (Continuum, Surelite, Santa Clara, CA) was passed through a third harmonic generator to produce 355 nm light (15 ns FWHM, 10 Hz). An excimer laser (Lambda Physik, XeCl, Ft. Lauderdale, FL) provided 308 nm light (20 ns FWHM, 5 Hz). Laser energies were measured with an energy meter (Scientech, #P09 joulemeter, Boulder, CO). The PA signal was detected using a 0.25 in. diameter, 5 MHz piezoelectric transducer (Panametrics, #A110S, Waltham, MA) and amplified (Panametrics, #5670, 100 × gain, or a Stanford Research Systems, #240, 5, 25, 125 × gain, Sunnyvale, CA) and collected using a digitizing oscilloscope (Lecroy, Chestnut Ridge, NY). Deconvolution of the experimentally acquired acoustic waveforms was accomplished using Sound Analysis 3000 (Quantum Northwest, Spokane, WA).

1.3. Description of capillary PA cell

The LPC described in detail elsewhere [18] was modified to provide a mechanism to couple the capillary tubing (Polymicro Technologies, 360 μm OD, 180 and 100 μm ID, Phoenix, AZ) to the piezoelectric transducer.

The modifications entail, first, using two Kalrez shims (Air Oil Products, Dupont #503N, Seattle, WA) to compress the capillary in between, and second, to fill the sample compartment of the LPC with distilled water or other coupling media as shown in Fig. 1.

Preparation of the quartz capillary cell requires pyrolysis[2] of about 1 cm of the polyamide coating on the 50 cm length of the capillary tubing to provide an optically transparent sample area. The optically transparent region of the tubing is centered and clamped in the LPC between two 0.030 in. Kalrez shims. Compression of the cell by an external clamp permits the Kalrez to form a gasket-tight fit around the capillary. A microliter gas tight syringe is attached to one end of the capillary tubing using a set of Microtight connectors (Upchurch, Oak Harbor, WA) in which an Upchurch F-185X microsleave is slipped over the 360 μm capillary tubing and the capillary assembly is inserted in to a M-110 minitight Kel-F fitting and tighten into a P-624 tefzel female luer. The capillary clamped in the center of the LPC was centered in the excitation source by adjusting the LPC in the *X–Y* plane until the shadow of the capillary as seen on an index card was centered in the beam.

1.4. PA signal amplitude versus pathlength

The LPC was assembled as previously described [18] (without a capillary) using various combinations of brass shims to provide pathlengths between 0.127–1.27 mm. The sample compartment of the LPC was filled with an aceto-

[1]High Pressure PA experiments have been used to obtain thermochemical information; see [21,22]. However to our knowledge no time-resolved studies have been reported.

[2]A micro torch can be used to burn off the coating.

nitrile solution of a PA standard, OHB, which had a calculated absorbance at 355 nm of 0.021 mm^{-1} or 0.044 mm^{-1}. The 355 nm laser line was attenuated and passed through an iris (5 mm diameter) to provide 240 μJ incident energy at the front of the LPC. The acoustic signal was detected with a 5 MHz piezoelectric transducer, amplified (Panametrics) and averaged on a digitizing oscilloscope.

1.5. Bp triplet quenching kinetics

For the time-resolved studies, the 355 laser line was attenuated to provide ca. 28 μJ energy incident upon a 180 μm ID capillary centered in the LPC. Two sets of solutions containing (1) Bp and (2) OHB (PA standard) were prepared in acetonitrile. Both solutions were diluted with a second stock water solution containing potassium iodide (KI) to yield a set of samples containing equivalent concentration of potassium iodide (KI) and maintaining matching optical densities (0.4 mm^{-1}) with a solvent composition of 9/1 acetonitrile/water. The samples were purged with nitrogen and charged into a gas tight 1000 μl syringe. Two to three datasets of data (R-wave (OHB), S-wave (Bp) and Background (KI/acetonitrile/water)) were collected at each KI concentration between 1 and 8 mM. The PA signal detected by the transducer was amplified 100 times (Panametrics) and averaged for 20–50 laser pulses using a digital oscilloscope. The excitation volume (V_0) in the quenching experiments is ca. 100 nl given a cross-sectional area of ca. 0.025 mm^2 and a length of 4 mm for the 180 μm ID capillary and the energy absorbed (H_{th}) by the sample is ca. 1000 nJ.

For the triplet energy determination measurement, low laser powers are required to avoid two photon artifacts. The 308 nm laser light was attenuated to provide ca. 5 μJ energy incident upon a 100 μm ID capillary centered in the LPC. Two solutions were prepared in aqueous acetonitrile with matching optical densities (0.35 mm^{-1} at 308 nm), one containing OHB and the other Bp. The signal from the transducer was amplified 500 times (SRS 240, 5× in series with the Panametrics, 100×) and averaged for 500 laser pulses using a digital oscilloscope. Nine waveforms (three R-wave, three S-wave and three solvent backgrounds) were collected and transferred to a PC for data analysis. The excitation volume (V_0) in the energy determination experiments is ca. 32 nl given a cross-sectional area of ca. 0.008 mm^2 and a length of 4 mm for the 100 μm ID capillary and the energy absorbed (H_{th}) by the sample is ca. 100 nJ.

2. Results and discussion

2.1. Properties of PA transient pressure changes

Absorption of electromagnetic radiation by a molecule generates an electronically and/or vibrationally excited state metastable intermediate. Heat released by nonradiative decay channels will yield a local increase in pressure (ΔP) that is proportional to the temperature rise (ΔT) as shown in Eq. (1),

$$\Delta P = \left(\frac{\beta}{\alpha}\right)\Delta T \tag{1}$$

where β is the thermal coefficient of expansion and α is the isothermal compressibility of the solvent. The temperature rise is proportional to the density of absorbed energy (H_{th}/V_0) and the thermoelastic properties of the solvent as shown in Eq. (2),

$$\Delta T = \left(\frac{H_{th}}{V_0}\right)\left(\frac{1}{C_p\rho}\right) \tag{2}$$

where H_{th} is the amount of absorbed photon energy released as heat, V_0 is the excitation volume, C_p is the heat capacity, and ρ is the density of the solvent. Eq. (3) shows the relationship between the heat released, H_{th}, and the energy

$$H_{th} = E_{lp}(1 - 10^{-A}) \tag{3}$$

of the excitation source, E_{1p}, where A is the absorbance of the sample. Substitution of Eq. (2) into Eq. (1) yields Eq. (4)

$$\Delta P = \left(\frac{H_{th}}{V_0}\right)\left[\left(\frac{\beta}{\alpha}\right)\left(\frac{1}{C_p\rho}\right)\right] \tag{4}$$

which shows that the photo-induced pressure rise is proportional to the thermoelastic properties of the solvent and the density of absorbed energy.

The amplitude of a PA signal resulting from local heating of the sample is proportional to the product of the photo-induced transient pressure change (ΔP) and a geometrical 'cell constant' (K) as shown in Eq. (5). The cell constant is a property of the

$$\text{Signal} \propto K^*\Delta P \tag{5}$$

geometry of the experiment and the mechanical to electrical conversion properties of the piezoelectric transducer and has been discussed in detail elsewhere [18,23].

Analysis of Eq. (4) permits an important distinction to be made between conventional transmission spectrophotometry and PA spectrophotometry. In the conventional experiment, the signal is proportional to the pathlength (Beer–Lambert Law). However, in the PA experiment, the signal is proportion to the density of absorbed energy, i.e., the energy absorbed by the sample in a given volume (H_{th}/V_0). At low absorbance, $A < 0.025$ cm^{-1}, H_{th} varies nearly linearly with the sample absorbance within our experimental error[3]. Therefore, the amplitude of the PA signal is assumed to be independent of the pathlength for an optically dilute sample. This independence results because of the absorbance, A, and the excitation volume, V_0, are proportional to the pathlength of the sample as shown in Eqs. (6) and (7)

[3] At higher A, the signal actually increases with decreasing pathlength, see Fig. 2, absorbance 0.044 mm^{-1}.

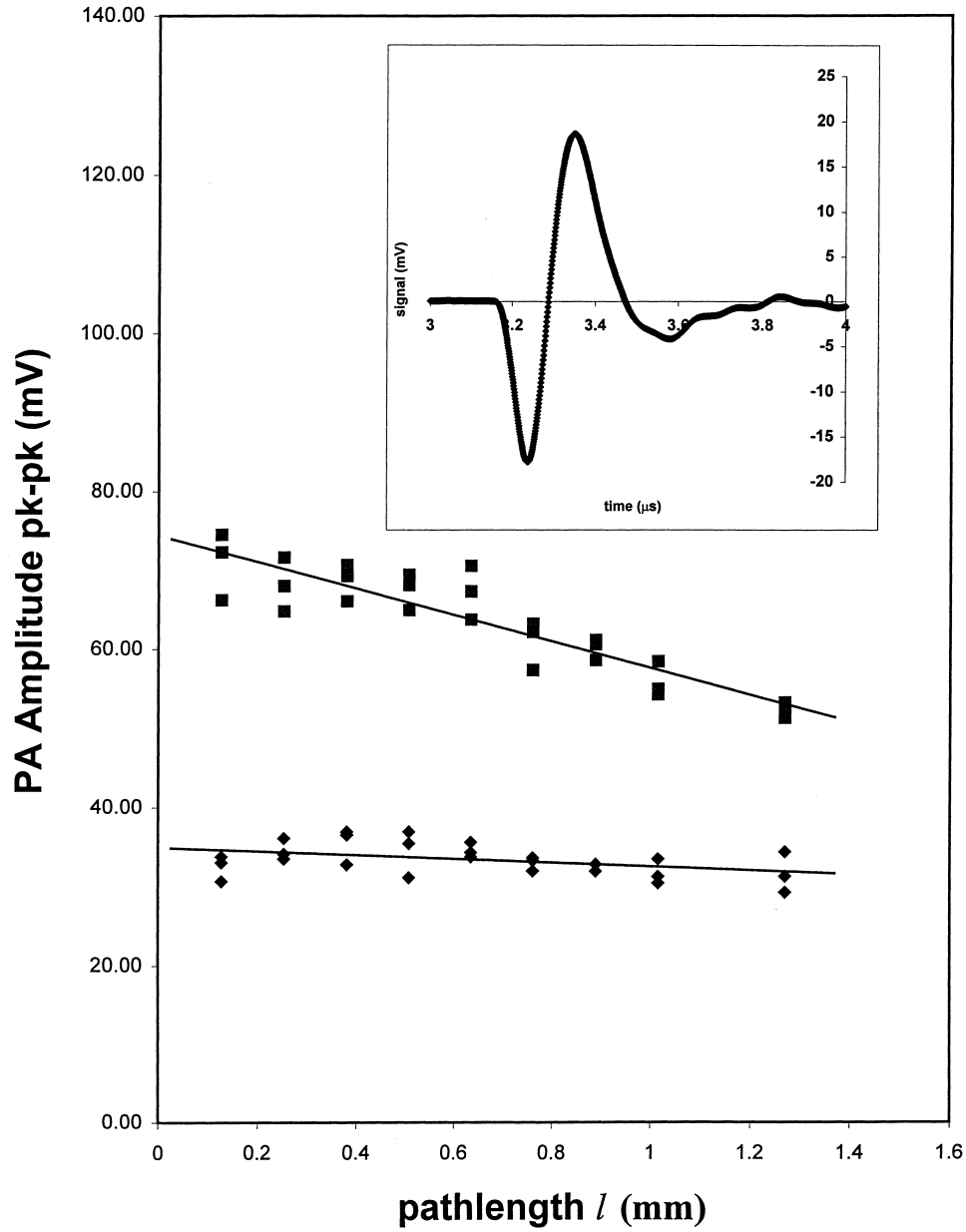

Fig. 2. Amplitude of the PA signal from OHB in acetonitrile as a function of pathlength in the LPC. <◆> OHB absorbance 0.021 mm^{-1}, <■>, OHB absorbance 0.044 mm^{-1}, 250 μJ incident light at 355 nm, 5 MHz transducer. Inset, PA waveform from LPC, 1.5 μJ absorbed energy in 2.5 μL volume.

where ϵ is the extinction coefficient and c is the concentration of the solute and r is the spatial radius of the laser beam and l is the pathlength.

$$A = \epsilon c l \tag{6}$$

$$V_0 = \pi r^2 l \tag{7}$$

This special feature of independence can be readily demonstrated with the LPC. The excitation volume, V_0, of the LPC can be varied by changing the pathlength of the sample cell, l, using various combinations of shims. Fig. 2 shows the amplitude of the PA signal obtained from irradiation of a PA standard (OHB, absorbance = 0.021 and 0.044 mm^{-1}) as a function of pathlength. Three experimental data points were obtained at each pathlength and were measured in random order. Thus the cell was taken apart and reassembled between each experiment. The scatter in the data demonstrates the importance of maintaining a constant cell geometry, specifically the position of the path of the laser beam relative to the piezoelectric detector. Using a cell clamped in place provides superior reproducibility with 1% RSD[4] for 20 individual experiments corrected for changes in laser power.

[4]%RSD = percent relative standard deviation = 100 × (the standard deviation of the samples) (average of the samples for 20 individual experiments corrected for changes in laser power).

The PA signal obtained from the 0.021 mm^{-1} OHB solution, shown in the Fig. 2 inset, demonstrates that densities of absorbed energy of near 1 μJ/μl lead to a readily measurable signal. The V_0 for a capillary cell (180 μm ID) is the cross-sectional area (ca. 0.025 mm^2) times the beam diameter of the laser (4 mm), which yields an excitation volume of $V_0 = 100$ nl. Therefore, even with moderate pulse energies, the FFSC should be capable of performing time-resolved PA experiments provided that (1) the excitation energy can be coupled into the sample and (2) the acoustic energy can be efficiently coupled from the sample to the acoustic detector.

Next, an approach to efficiently couple the light into the fused capillary cell and couple the acoustic signal to the piezoelectric detector is outlined. Finally, the time-resolved capabilities are demonstrated by measuring both the excited state energy and lifetime of Bp triplet in the presence and absence of a quencher.

2.2. Description of the FFSC PA cell

The LPC was used as a 'light guide' to bring the excitation energy to the capillary cell and as an 'acoustic guide' to transfer the pressure pulse from the capillary cell to the detector. Fig. 1 shows a schematic of the FFSC housed within the LPC. A critical parameter for this arrangement is the choice of the fluid coupling media used in the compartment of the LPC surrounding the capillary tubing. Obviously the media should have minimum absorption at the excitation wavelength, however, a more subtle property is the acoustic impedance of the coupling fluid.

2.3. Coupling media

The coupling media is defined as the fluid used in the cavity of the LPC. Traditionally, the cavity of the layered prism cell is where the sample is contained, however in the capillary PA cell, the fluid is chosen to provide a media to transfer the acoustic signal from the sample to the detector.

Comparison of the acoustic waveforms obtained from irradiation of the PA standard, (OHB), using water and benzene as the coupling fluid provides two notable observations. First, when water is used as the coupling fluid, the acoustic waveform arrives at the detector 70 ns before the acoustic waveform obtained when benzene was used as the coupling fluid. Second, when water is used as the coupling fluid, the amplitude of the acoustic waveform is 40% greater than the signal observed when the coupling fluid was benzene.

The first observation, the difference in arrival times, is due to the difference in the speed of sound between the two coupling media. Using literature values for the speed of sound in the two media [24] and the distance the acoustic wave travels through the media, an estimate of the difference in arrival times ($\Delta t = 70 \pm 10$ ns) can be calculated as shown in Eq. (8), where $(d - r_{cap})$ is the thickness of the fluid layer, d is the thickness of the shim (762 ± 8 μm),

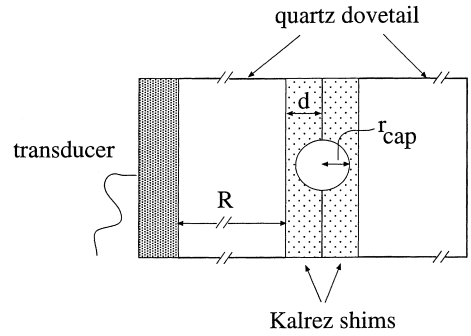

Fig. 3. Cross-section view of FFSC compressed between a pair of Kalrez shims, d is the thickness of the shim (762 μm), r_{cap} is the radius of the silica capillary (90 μm), and R is the thickness of the prism.

$$\Delta t = \frac{(d - r_{cap})}{[v_{H_2O} - v_{PhH}]} \quad (8)$$

r_{cap} is the internal radius of the capillary tubing (90 ± 5 μm), see Fig. 3, v_{H_2O} is the velocity of sound in water (1.497 mm/μs) and v_{PhH} is the velocity of sound in benzene (1.295 mm/μs). The value calculated from Eq. (8) (70 ± 10 ns) compares well with the experimentally observed Δt of 70 ns.

The second observation, the enhanced signal amplitude with water as a coupling fluid, is likely due to the associated acoustic coupling losses as the sound wave propagates through the multiple layers. Acoustic coupling losses are described in terms of the acoustic impedance, Z, defined as the product of the speed of sound (m/s) in the media and the density of the media (Kg/m^3). Comparison of the relative acoustic impedance for a quartz/solvent/quartz series should provide insight into the observed difference in signal amplitude. Using this as a criteria, ca. 1.5 times the signal amplitude is expected using water as the acoustic coupling fluid since the fraction of acoustic energy (f) transferred from the capillary quartz tubing/fluid interface/quartz prism is ca. 13% for water and 9% for benzene is shown in Eq. (9), where Z_1 is the acoustic impedance of quartz and Z_2 is the acoustic impedance of the coupling fluid and f^2 accounts for a three layer symmetric impedance boundary.

$$f^2 = \left[1 - \frac{(Z_1 - Z_2)^2}{(Z_1 + Z_2)^2}\right]^2 \quad (9)$$

Although the radial geometry of the capillary is not the optimum[5], the high sensitivity of the PA method provides experimental flexibility. Specifically, the benefits of an experimental approach to obtain calorimetric and kinetic information on nanoliters of sample with simple and inexpensive materials outweighs the lack of an optimum geometry.

[5]For a cylindrical source the amplitude of the acoustic wave decreases inversely with distance between the excitation source and detector. A geometry that yields a planar acoustic wave, e.g., the layered cells is discussed in [10,11,18].

2.4. Time-resolved calorimetry

Recently the benefits of the LPC geometry in PA analysis have been described in detail [18]. The absence of a background signal due to cell absorbance in the LPC geometry provides an experimental approach to measure the kinetics of photo-generated intermediates, generated in optically dilute solutions. To demonstrate the ability to measure the dynamics (kinetics and thermodynamics) of photo-induced reaction pathways using the capillary cell, we examined the lifetime of triplet benzophenone (Bp^{*3}) in the presence and absence of a quencher, potassium iodide (KI).

Irradiation of an air-saturated solution of Bp results in the prompt (10 ps) [25] and efficient ($\varphi = 1.0$) [26] formation of the excited state triplet metastable intermediate Bp^{*3} (Eqs. (10) and (11)).

$$Bp + h\nu \rightarrow Bp^{*1} \quad (10)$$

$$Bp^{*1} \rightarrow Bp^{*3} \quad (11)$$

Comparison of the PA waveform obtained from irradiation of Bp and OHB in the 100 μm capillary cell is shown in Fig. 4. Deconvolution of the Bp data provides a triplet energy of ca. 69.5 ± 1.4 kcal/mol which is within the experimental error of the reported literature value 69.2 kcal/mol [27].

In the presence of potassium iodide (KI), the triplet excited state (Bp^{*3}) is quenched by an electron transfer mechanism [28] to yield ground state Bp plus heat (Δ), Eq. (12).

$$Bp^{*3} + KI \xrightarrow{K_q} Bp + \Delta \quad (12)$$

As expected, addition of KI (1–8 mM) to the Bp sample decreases the observed lifetime (τ_{obs}) of Bp^{*3}. The rate of

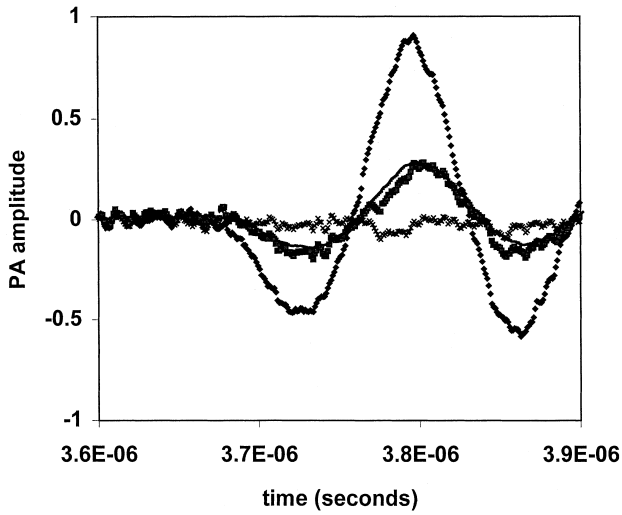

Fig. 4. Comparison of the PA waveform (5 MHz transducer) obtained from irradiation of an air saturated solution of Bp and OHB in the 100 μm fused silica capillary. <◆> OHB, <■> Bp, and <x> residuals. <———> shows the calculated fit provided an experimental measure for BP^{*3} of 69.5 ± 1.4 kcal/mol.

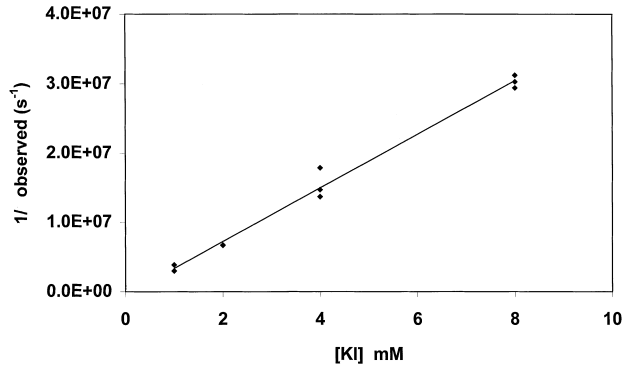

Fig. 5. A plot of 1/τ observed versus potassium iodide (KI) concentration. Linear regression yields a quenching rate constant of $(3.9 \pm 0.2) \times 10^9\ M^{-1}\ s^{-1}$ for Bp^{*3} quenching by KI.

triplet quenching calculated from the slope of a plot of $1/\tau_{obs}$ versus [KI] (Fig. 5) was $3.9 \pm 0.2 \times 10^9\ M^{-1}\ s^{1}$.

3. Conclusions

Using a nano-scale PA cell made from flexible fused silica quartz capillary tubing, we demonstrated the ability to obtain both kinetic and thermodynamic data with minute quantities of sample (100 nl volume). We have shown how the layered prism cell can be modified to (1) couple the excitation energy in to the sample and (2) couple the acoustic signal to a piezoelectric detector.

Two considerations for choice of coupling fluid used in the LPC were found to be important: (1) absorptivity and (2) acoustic coupling. Benzene was considered initially as a coupling fluid to permit greater coupling of the excitation light through capillary tubing given the refractive index match between benzene and quartz. However, water was found to be a better coupling fluid given its enhanced acoustic coupling to the quartz components of the PA cell and minimal absorption in the UV–VIS region.

Not only does the narrow-bore flexible fused silica quartz capillary provide an experimental approach to investigate the kinetics and thermodynamics of reactive intermediates on a nano-scale, it may also provide the ability to perform PA experiments at mega-pressures. One of our primary interests in the capillary cell stems from the success of the capillary tubing in high pressure NMR studies where pressure up to 60,000 PSI are obtainable with the 100 μm ID tubing [20]. Work is in progress to utilize the flexible fused silica quartz capillary tubing PA cell in a high pressure mode to investigate the kinetic and thermodynamic properties of metal carbonyl C–H bond activation.

Acknowledgements

This work was supported by the US Department of Energy, Office of Basic Energy Research, Chemical

Sciences Division, Process and Techniques Branch. The work was conducted at Pacific Northwest Laboratory, which is operated by Battelle Northwest for the US Department of Energy under Contract DE-ACO6-76RL0 1830. Support for NE and KK was provided through AWU-NW under Grant DE-FGO6-89ER-75522 with the US Department of Energy. TA thanks Drs. Clem Yonker and Tom Zemanian for sharing their high pressure luer fittings and discussions relating to the preparation of fused silica capillary tubing for optical studies and Professor Jeanne Small at EWU for a critical review of this paper.

References

[1] S.E. Braslavsky, G.E. Heibel, Time-resolved photothermal and photoacoustic methods applied to photoinduced processes in solution, Chem. Rev. 92 (1992) 1381–1410.
[2] R.A. Caldwell, D.J. Unett, J.J. Vipond, Time-resolved photoacoustic calorimetry of tri- and tetraphenylethylenes. Do S0 and T1 energy surfaces cross?, Photochem. Photobiol. 65 (1997) 530–534.
[3] J. Feitelson, D. Mauzerall, Photoacoustic evaluation of volume and entropy changes in energy and electron transfer. Triplet state porphyrin with oxygen and naphthoquinone-2-sulfonate, J. Phys. Chem. 100 (1996) 7698–7703.
[4] I.R. Gould, J.E. Moser, B. Armitage, S. Farid, J.L. Goodman, M.S. Herman, Electron transfer reactions in the marcus inverted region, J. Am. Chem. Soc. 111 (1989) 1917–1919.
[5] L.J.J. Laarhoven, P. Mulder, α-C–H bond strengths in tetralin and THF: application of competition experiments in photoacoustic calorimetry, Phys. Chem. B 101 (1997) 73–77.
[6] S. Malkin, The photoacoustic method in photosynthesis – monitoring and analysis of phenomena which lead to pressure changes following light excitation, Adv. Photosynth. 3 (1996) 191–206.
[7] K.S. Peters, Time-resolved photoacoustic calorimetry: from carbenes to proteins, Angew. Chem. Int. Ed. Engl. 33 (1994) 294–302.
[8] D.D.M. Wayner, E. Lusztyk, D. Page, K.U. Ingold, P. Mulder, L.J.J. Laarhoven, H.S. Aldrich, Effects of solvation on the enthalpies of reaction of tert-butoxyl radicals with phenol and on the calculated 0–H bond strength in phenol, J. Am. Chem. Soc. 117 (1995) 8737–8744.
[9] T.J. Burkey, M. Majewski, D. Griller, Heats of formation of radicals and molecules by a photoacoustic technique, Am. Chem. Soc. 108 (1986) 2218–2221.
[10] L.A. Melton, T. Ni, L. Qingzheng, Photoacoustic calorimetry: a new cell design and improved analysis algorithms, Rev. Sci. Instrum. 60 (1989) 3217–3223.
[11] O.V. Puchenkov, Z. Kopf, S. Malkin, Photoacoustic diagnostics of laser-induced processes in reaction centers of Rhodobacter sphaeroides, Biochim. Biophys. Acta 1231 (1995) 197–212.
[12] J.R. Small, L.J. Libertini, E.W. Small, Analysis of photoacoustic waveforms using the nonlinear least squares method, Biophys. Chem. 42 (1992) 29–48.
[13] J.E. Rudzki, J.L. Goodman, K.S. Peters, Simultaneous determination of photoreaction dynamics and energetics using pulsed, time-resolved photoacoustic calorimetry, J. Am. Chem. Soc. 107 (1985) 7849–7854.
[14] R. Klenze, J.I. Kim, A direct speciation of transuranium elements in natural aquatic systems by laser-induced photoacoustic spectroscopy, Radiochim. Acta 44/45, 77–85 (1988).
[15] S. Okajima, D.T. Reed, J.V. Beitz, C.A. Sabau, D.L. Bowers, Speciation of Pu(VI) in near-neutral solutions via laser photoacoustic spectroscopy, Radiochim. Acta 52/53, (1991) 111–117.
[16] N.S. Foster, J.E. Amonette, T. Autrey, In situ detection of chromate using photoacoustic spectroscopy, Applied Spec. 5, 3(6) (1999).
[17] L.G. Arnaut, R.A. Caldwell, J.E. Elbert, L.A. Melton, Recent advances in photoacoustic calorimetry: theoretical basis and improvements in experimental design, Rev. Sci. Instrum. 63 (1992) 5381–5389.
[18] T. Autrey, N.S. Foster, K. Klepzig, J.E. Amonette, J.L. Daschbach, A new angle into time-resolved photoacoustic spectroscopy: a layered prism cell increases experimental flexibility, Rev. Sci. Instrum. 69 (1998) 2246–2258.
[19] J.D. Spear, G.L. Klunder, R.E. Russo, Photothermal deflection spectroscopy of an aqueous sample in a narrow bore quartz capillary, Rev. Sci. Instrum. 69 (1998) 2259–2267.
[20] J.C. Linehan, S.L. Wallen, C.R. Yonker, T.E. Bitterwolf, J.T. Bays, In situ NMR observations of the photolysis of cymantrene and mehtylcymantrene in supercritical fluids: a new technique using high pressure NMR, J. Am. Chem. Soc. 119 (1997) 10170–10177.
[21] E.F. Walsh, M.W. George, S. Goff, S.M. Nikiforov, V.K. Popov, X.-Z. Sun, M. Poliakoff, Energetics of the reactions of $(n_6\text{-}C_6H_6)Cr(CO)_3$ with *n*-Heptane, N_2, and H_2 studied by high-pressure photoacoustic calorimetry, J. Phys. Chem. 100 (1996) 19425–19429.
[22] E.F. Walsh, V.K. Popov, M.W. George, M. Poliakoff, Photoacoustic calorimetry at high pressure: a new approach to determination of bond strengths. estimation of the M-L bond dissociation energy of $M(CO)_5L$ (M = Cr, Mo; L = H_2, N_2) in *n*-Heptane solution, J. Phys. Chem. 99 (1995) 12016–12020.
[23] S.E. Braslavsky, K. Heihoff, Photothermal methods, in: J.C. Scaiano (Ed.), Handbook of Organic Photochemistry, CRC Press, Boca Raton, 1989, p. 327–355.
[24] R.C. Weast, Handbook of Chemistry and Physics, 63rd ed., CRC Press, Boca Raton, 1982.
[25] B.I. Green, R.M. Hochstrasser, R.B. Weisman, Picosecond transient spectroscopy of molecules in solution, J. Chem. Phys. 70 (1979) 1247–1259.
[26] A.A. Lamola, G.S. Hammond, Mechanisms of photochemical reactions in solution XXXIII. Intersystem crossing efficiencies, J. Chem. Phys. 43 (1965) 2129–2135.
[27] S.L. Murov, I. Carmichael, G.L. Hug, Handbook of Photochemistry, 2nd ed., Marcel Dekker, New York, 1993.
[28] H. Shizuka, H. Obuchi, Anion-induced triplet quenching of aromatic ketones by nanosecond laser photolysis, J. Phys. Chem. 86 (1982) 1297–1302.